Effective spectral optical functions of lamellar nanogratings

Martin Foldyna
marfol@gmail.com
Laboratory of Physics of Interfaces and Thin Films, Ecole Polytechnique, Route de Saclay, 91128 Palaiseau Cedex, France

Kamil Postava
kamil.postava@vsb.cz
Department of Physics, Technical University of Ostrava, 17. listopadu 15, 708 33 Ostrava–Poruba, Czech Republic
Laboratory of Magnetism, Institute of Experimental Physics, University of Bialystok, 41 Lipowa Street, 15-424 Bialystok, Poland

Razvigor Ossikovski
razvigor.ossikovski@polytechnique.edu
Laboratory of Physics of Interfaces and Thin Films, Ecole Polytechnique, Route de Saclay, 91128 Palaiseau Cedex, France

Antonello De Martino
martino@leonardo.polytechnique.fr
Laboratory of Physics of Interfaces and Thin Films, Ecole Polytechnique, Route de Saclay, 91128 Palaiseau Cedex, France

Enric Garcia-Caurel
enric.garcia-caurel@polytechnique.edu
Laboratory of Physics of Interfaces and Thin Films, Ecole Polytechnique, Route de Saclay, 91128 Palaiseau Cedex, France

Spectral properties of lamellar sub-wavelength gratings (nanogratings) are described by effective medium approximation (EMA). Analytical spectral formulae for ordinary and extraordinary effective optical functions are derived for nanogratings consisting of material described by Sellmeier, damped harmonic oscillator, and Drude formulae. Spectral origin for birefringence of dielectric nanogratings and linear dichroism for absorbing ones is discussed for model cases and gratings consisting of real natural materials. Simple approximation by zero-order diffraction is compared with rigorous modeling based on Rigorous Coupled Wave Analysis (RCWA). Limits of applicability of effective medium approximation is discussed in the spectral domain. [DOI: 10.2971/jeos.2006.06015]

Keywords: Diffraction gratings, nanogratings, effective medium approximation, spectral optical functions, anisotropic optical materials

1 Introduction

Optical methods represented by reflection and transmission spectroscopy, ellipsometry, and polarimetry became nowadays standards of process monitoring and quality control in semiconductor technology. New trends in ultra large scale integrated circuits require adaptation of optical methods for nondestructive characterization and control of lithographic and nanostructurization processes.

Successful implementation and sub-nanometer sensitivity of optical methods are conditioned by their application in a wide spectral range [1, 2]. The main advantage of spectral measurement is fitting of data to an appropriate model consisting of a few unknown parameters. Complex spectral optical properties are described by model dielectric functions consistent with microscopic mechanisms of spectral absorption and fulfilling the Kramers-Kronig dispersion relations [3]. Consequently, there is a need for detailed study of optical properties of periodic gratings and nanosystems in spectral domain.

On the other hand, the sub-wavelength gratings behave as effective media with artificial optical properties, which have no analogy among natural materials. Symmetry reduction by nanostructurization results in a strong form anisotropy and gives possibility to apply nanogratings as polarizing devices. Recently, a birefringent quarter wave plate [4], polarizing beam-splitters [5], and other quasi-achromatic polarizing devices designed from dielectric gratings [6] have been reported. Detail understanding of device functionality requires knowledge of spectral properties of such periodic systems.

Modeling of optical properties of gratings and periodic systems is usually based on generalization of the Berreman matrix approach used for anisotropic multilayer systems [7]. For laterally periodic systems the rigorous coupled wave analysis (RCWA) applies truncated Fourier series expansions for description of the electromagnetic field in the structure [8, 9]. Compared to the multilayer models, the RCWA computing is much more time consuming, which becomes a problem particularly for spectral modeling and fitting.

One from the approaches to simplify modeling of the sub-wavelength gratings is to use the effective medium approximation (EMA), which replaces grating by an effective layer with new optical parameters. Effective parameters of isotropic lamellar gratings were intensively studied in the single wavelength context and optical constants of the effective layer in quasi-static limit (ratio between the grating period Λ and the incident light wavelength λ is close to zero) are very well known [10].

Received July 24, 2006; published September 18, 2006 ISSN 1990-2573

Expressions for the isotropic gratings and detailed study of the validity of different EMA approaches were presented by Haggens, Li, and Kostuk [11]. Moreover, the authors proposed approach which is based on exact Bloch wave numbers and provides very good description for dielectric gratings. The case of metallic grating was shown to be more complicated as the assumptions justifying EMA are broken generally for much smaller values of Λ/λ. Necessity to obtain exact wave numbers makes this solution rather precise, but unfortunately time consuming.

That approach is principally different from original work of Rytov [12], where approximate analytical formulae were obtained directly from the Maxwell equations under the condition of normal incidence. The theory was generalized and precised later by Lalanne and Hugonin [13], where rather complicated expressions are presented providing very precise values of effective parameters. Recently, quasi-static expressions for the generally anisotropic lamellar gratings were reported in Ref. [14].

This paper deals with description of lamellar nanogratings by spectral effective medium approximation. Simple analytical formulae in quasi-static limit are compared with rigorous modeling based on RCWA. Our approach is demonstrated on nanogratings consisting of typical representative materials: a dielectric dispersive medium (SiO_2), an absorbing material with interband electronic transitions (Si), and a metal with typical free electron absorption (Ag).

Basic theory and procedure to obtain effective parameters of nanogratings is presented in Section 2. The quasi-static approximation of EMA is applied on elementary optical functions in Section 3. Spectral origin of interesting birefringent and dichroic properties of nanogratings is explained on example of three basic optical functions: Sellmeier relation describing dispersion in non-absorbing spectral range, damped harmonic oscillator describing absorption, and Drude model for free electron absorption in metals. Section 4 deals with real natural materials and the simple EMA is compared with rigorous RCWA modeling. Limits and applicability of the approximation are discussed.

2 THEORY

2.1 Formulation of the problem

Figure 1 shows the geometry of the binary lamellar grating and the coordinate system used in this article. Incident light is assumed in the form of a monochromatic plane wave with wave vector in the plane yz. For simplicity we restrict our description and modeling to gratings consisting of isotropic materials. Incident light is assumed in the form of a monochromatic plane wave with time dependence described by factor $\exp(-i\omega t)$, where ω is the angular frequency. Wave vector is chosen to be parallel to the plane yz.

According to the Floquet theorem, the electromagnetic field in the periodic structure shown in Figure 1 can be described using a periodic functions of the in-plane space coordinates. Moreover, the electric and magnetic fields **E** and **H** in the grating can be expressed after suppressing time dependence in the forms

$$\mathbf{E}(\mathbf{r}) = \sum_m \exp(i\mathbf{k}_m \cdot \mathbf{r}) \sum_n A^E_{mn} \mathbf{e}_m \exp(iny2\pi/\Lambda), \quad (1a)$$

$$\mathbf{H}(\mathbf{r}) = \sum_m \exp(i\mathbf{k}_m \cdot \mathbf{r}) \sum_n A^H_{mn} \mathbf{h}_m \exp(iny2\pi/\Lambda), \quad (1b)$$

where $\mathbf{k}_m = [k_{x,m}, k_{y,m}, k_{z,m}]$ denotes the Bloch wave vector for given wavelength λ, A^E_{mn} and A^H_{mn} denote the amplitudes of n-th Fourier harmonics of m-th Bloch wave. Vectors $\mathbf{e}_m$ and $\mathbf{h}_m$ denote the polarization vectors of m-th Bloch wave.

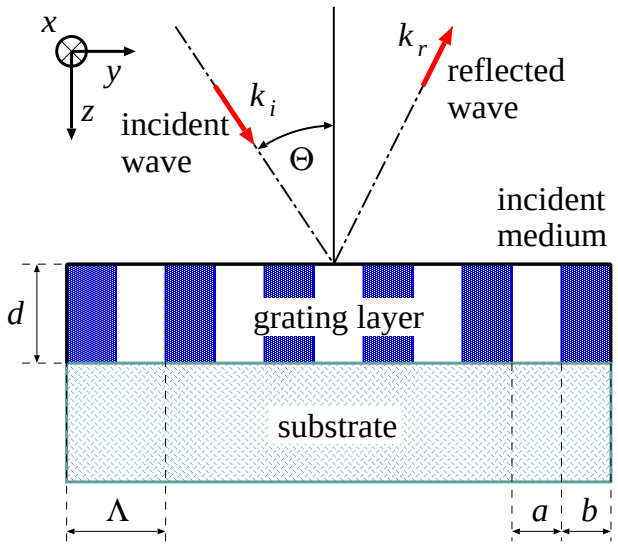

FIG. 1 Structure with one-dimensional lamellar grating layer. In terms of the grating period Λ, the fill factor is defined as $f = a/\Lambda$.

The Maxwell equations can be after suppressing periodic time dependence (and assuming permeability has its vacuum value) written in the normalized form

$$\nabla \times \mathbf{H}(\mathbf{r}) = -ik_0 \varepsilon_R(\mathbf{r}) \mathbf{E}(\mathbf{r}), \quad (2a)$$

$$\nabla \times \mathbf{E}(\mathbf{r}) = ik_0 \mathbf{H}(\mathbf{r}), \quad (2b)$$

where $\varepsilon_R(\mathbf{r})$ denotes the relative permittivity in the grating layer and $k_0 = 2\pi/\lambda$.

Eqs. (2a) and (2b) can be solved by the RCWA [8, 9], which converts these equations into the eigenvalue problem resulting in the Bloch wave numbers $k_{z,m}$ and eigenvectors describing spatial dependence of Bloch waves in xy plane. Special care should be taken with expressing permittivity tensor by using truncated Fourier series as it significantly influences precision of the results. At this stage of algorithm the boundary conditions are included also in the representation of the permittivity tensor. If Li factorization rules [15] are used for lamellar grating, the zero order Bloch wave in nanograting corresponds in first approximation to a plane wave with wave number of the zero Fourier harmonic [14] (this wave number can be obtained by assuming expansion with only zero Fourier harmonic – quasi-static limit).

For coupling the field in the incident medium and the substrate, the boundary conditions are applied, which state that

the tangential components of the electric and magnetic field as well as normal components of electric displacement and magnetic flux density have to be continuous on each interface. Stable implementation of the boundary conditions is provided by S-matrix algorithm [16], which respects direction of propagation of the Fourier harmonics. Numerically it means to avoid propagation matrices containing simultaneously exponentially increasing and decreasing elements.

2.2 Effective medium approximation

Effective medium approximation is used in the cases if the grating has period Λ much smaller then the wavelength of the incident light $\Lambda \ll \lambda$. In the frame of this theory, the grating layer is replaced by an effective homogeneous anisotropic layer, which describes optical properties of the original grating. Precision of this description depends on the Λ/λ ratio, but also on the way the effective parameters are obtained.

In this article two types of description of the effective layer are used:

(i) analytical EMA values for quasi-static cases ($\Lambda/\lambda \to 0$) and

(ii) EMA values obtained from fit of the rigorous RCWA data ($\Lambda/\lambda \ll 1$).

In quasi-static limit, parameters of the layer can be expressed in the simple form either for isotropic [11] or for anisotropic gratings [14]. Nanogratings consisting of isotropic materials $\epsilon^{(H)}$ (lamellas) and $\epsilon^{(L)}$ (inter-lamellar medium) are represented as uniaxial effective media described by the ordinary and extraordinary effective permittivities ϵ_o and ϵ_e in the form [11]:

$$\epsilon_o = f\epsilon^{(H)} + (1-f)\epsilon^{(L)},\ \epsilon_e = \frac{\epsilon^{(H)}\epsilon^{(L)}}{f\epsilon^{(L)} + (1-f)\epsilon^{(H)}}, \qquad (3)$$

where $f = a/\lambda$ denotes the fill factor.

It is worthy to remark here that these expressions can be obtained from matrix representing Fourier expansion of the permittivity tensor, where the necessary condition is correct application of the Li factorization rules. The reason for this simple relation is that zero-order TE and TM polarized Bloch modes can be in quasi-static limit approximately described by plane waves with wave numbers, which are directly related to ordinary and extraordinary refractive indices. At the same time, when factorization rules are applied in rigorous modeling, zero Fourier harmonics directly correspond to these Bloch waves.

Beyond the quasi-static area there is still the possibility to describe sub-wavelength gratings by using homogeneous anisotropic layers. Despite that the simple analytical formulae cannot be provided in some cases, there is still possibility to obtain approximate expressions for effective parameters [11]-[13]. Nevertheless, to avoid any inaccuracy by choosing approximate model, following procedure to fit the rigorous data is used in this article.

Optical response of a grating described by Mueller matrices is modeled by using the RCWA. Rigorous data for incidence angles ranging from 0° to 80° with step of 5° are fitted by uniaxial effective medium. For spectral response we fit each wavelength separately. The fitting approach allows to obtain information of the quality of description of the nanograting by the EMA and magnitude of dependence of the effective parameters on the incidence angles. The information is obtained as an error of the nonlinear fit by Levenberg–Marquardt method.

3 MODELING OF SPECTRAL OPTICAL FUNCTIONS

This section deals with application of simple EMA [Eq. (3)] to basic dispersion formulae describing wavelength or energy dependence of the complex optical functions. The most representative dispersion optical functions are Sellmeier, damped harmonic oscillator (DHO), and Drude functions, which are introduced and discussed.

3.1 Sellmeier formula

In visible spectra many dielectrics are non-absorbing and their dispersion can be described by the Sellmeier optical functions in the form:

$$\epsilon(E) = \epsilon_0 + \frac{AE_1^2}{E_1^2 - E^2}, \qquad (4)$$

where the constants ϵ_0, A, and E_1 represent the non-dispersive term, the amplitude, and the energy of the absorption peak outside the parametrized range, respectively.

Now let us consider a grating consisting of lamellas from dielectric material $\epsilon^{(H)}$ described using Sellmeier spectral dependence (4) embedded in air $\epsilon^{(L)}(E) = 1$. The grating can be represented using effective medium with ordinary and extraordinary permittivities also in the Sellmeier form:

$$\epsilon_o(E) = \epsilon_{0,o} + \frac{A_o E_{1,o}^2}{E_{1,o}^2 - E^2},\ \epsilon_e(E) = \epsilon_{0,e} + \frac{A_e E_{1,e}^2}{E_{1,e}^2 - E^2}, \qquad (5)$$

where constants ϵ_o, A_o, $E_{1,o}$, ϵ_e, A_e, and $E_{1,e}$ can be found in the second column of the Table 1. Therefore, sub-wavelength gratings from Sellmeier material behave as uniaxial material whose ordinary and extraordinary optical functions can be described also by Sellmeier formulae with generally different parameters, depending on the fill factor of the grating f.

Figure 2 shows an example of spectral dependence of effective optical functions of nanograting from a dielectric material similar to SiO_2. Chosen values of parameters are $\epsilon_0 = 1$, $A = 1.098$, and $E_1 = 13.36$ eV. Effective optical properties increases with increasing fill factor f, which corresponds to effective mixture of grating material with air. Note that for extraordinary permittivity also the resonant Sellmeier frequency $E_{1,e}$ is shifted to higher energies, which corresponds to birefringence of dielectric nanogratings.

Figure 3 shows the birefringence $\Delta n = n_o - n_e$ as a function of the fill factor f. Ordinary and extraordinary refractive indices can be obtained as the square roots of corresponding

permittivities. One can see that ordinary permittivity is larger for all fill factors than extraordinary, where the highest difference is around fill factor of 0.5. This behaviour is typical for all sub-wavelength gratings from loss-less materials (not only those described by Sellmeier formulae). Clearly for the limiting cases $f = 0$ and $f = 1$ the effective medium is isotropic.

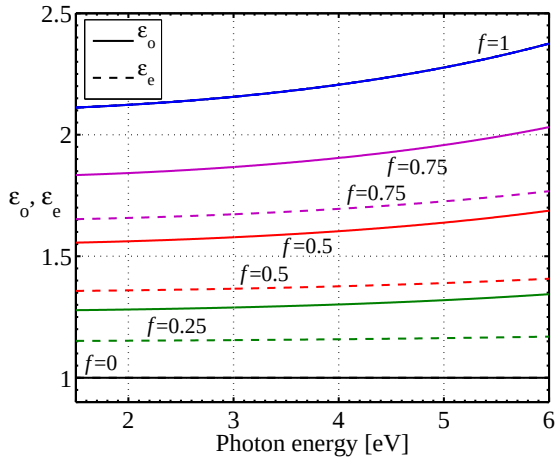

FIG. 2 Modelled Sellmeier spectral dependencies of the ordinary (solid lines) and extraordinary (dashed lines) permittivity on the light energy are shown for different fill factors f. Material of lamellas is characterized by the parameters $\epsilon_0 = 1$, $A = 1.098$, and $E_1 = 13.36$ eV from Eq. (4).

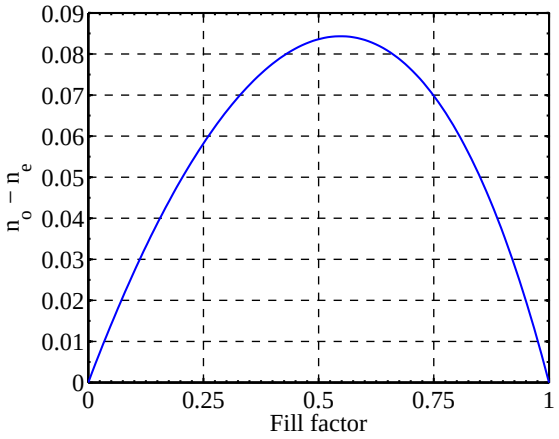

FIG. 3 Birefringence of nanograting $\Delta n = n_o - n_e$ as a function of the fill factor f for the energy 2 eV. Other parameters are the same as for Figure 2

3.2 Damped harmonic oscillator

Another model very often used for description of broadened absorption spectral line is the damped harmonic oscillator (DHO). It often originates from interband electronic transitions in visible and ultraviolet spectral range, or from resonant vibration transitions in infrared region. Spectral dielectric function of DHO is usually expressed in the form:

$$\epsilon(E) = \epsilon_0 + \frac{AE_0^2}{E_0^2 - E^2 - i\Gamma E_0 E}, \tag{6}$$

where A is the amplitude, E_0 is the Lorentz resonant frequency, and Γ is the broadening parameter of harmonic oscillator. Note that for negligible broadening $\Gamma = 0$, the DHO optical response reduces to Sellmeier function (4).

Using EMA formulae from (3) with $\epsilon^{(H)}$ from Eq. (6) and $\epsilon^{(L)}(E) = 1$ leads to the following formulae for new DHOs:

$$\epsilon_o(E) = \epsilon_{0,o} + \frac{A_o E_{0,o}^2}{E_{0,o}^2 - E^2 - i\Gamma_o E_{0,o} E}, \tag{7a}$$

$$\epsilon_e(E) = \epsilon_{0,e} + \frac{A_e E_{0,e}^2}{E_{0,e}^2 - E^2 - i\Gamma_e E_{0,e} E}, \tag{7b}$$

Expressions for parameters $\epsilon_{0,o}$, A_o, $E_{0,o}$, Γ_o, $\epsilon_{0,e}$, A_e, $E_{0,e}$, and Γ_e can be found in the third column of the Table 1.

Both, ordinary and extraordinary effective functions of DHO are described in quasi-static limit also by the DHO functions. As Figure 4 shows for parameters $\epsilon_0 = 1$, $A = 3$, $E_0 = 3$ eV, and $\Gamma = 0.25$, ordinary optical function only changes amplitude with respect to the fill factor (linear combination of two materials $\epsilon^{(H)}$ and $\epsilon^{(L)}$). On the other hand, effects in the extraordinary optical function are much more interesting. Peak in the imaginary part is shifted to the higher energies, where the shift and also amplitude depend on the fill factor. Due to the Kramers-Kronig relations, also the real part of extraordinary permittivity changes, following changes in the peak position.

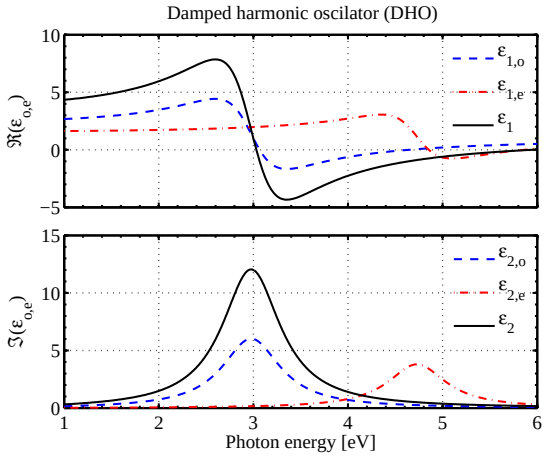

FIG. 4 Real ϵ_1 and imaginary ϵ_2 part of permittivity as dependence on spectral energy for nanograting consisting of lamellas modelled using DHO optical function (6) with parameters $\epsilon_0 = 1$, $A = 3$, $E_0 = 3$ eV, and $\Gamma = 0.25$. Dashed and dash-dotted lines correspond to the effective ordinary and extraordinary optical functions for the fill factor $f = 0.5$, respectively.

The Lorentz resonant frequency $E_{0,e}$ as well as broadening parameter Γ_e are shown in Figure 5. Significant shift of the resonant frequency to higher energies for decreasing fill factor is demonstrated. Products $\Gamma_o E_{0,o}$ and $\Gamma_e E_{0,e}$ are always constant, which means that spectral broadening of peaks remain constant for all fill factors for both ordinary and extraordinary optical functions.

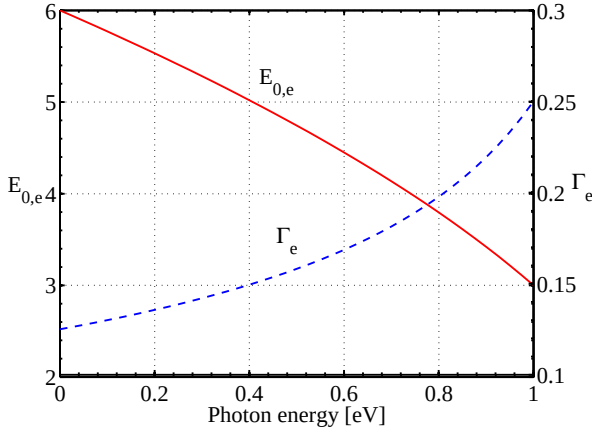

FIG. 5 Dependence of the extraordinary optical function parameters $E_{0,e}$ and Γ_e on the fill factor is shown. Other parameters are the same as for Figure 4.

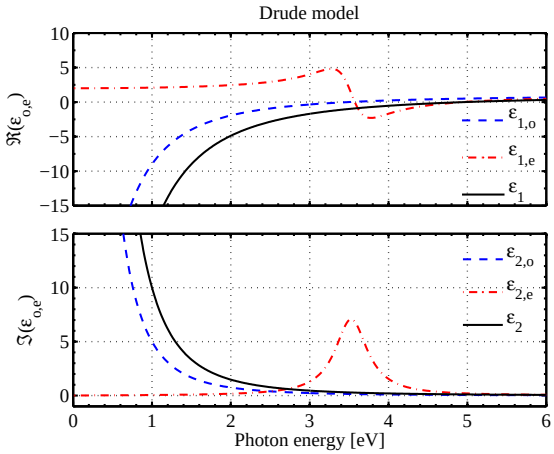

FIG. 6 Real ϵ_1 and imaginary ϵ_2 part of permittivity as dependence on the photon energy for nanograting consisting of lamellas modelled using Drude optical function (8) with parameters $\epsilon_0 = 1$, $A = 5$ eV, and $\Gamma = 0.5$ eV (solid lines). Dashed and dash-dotted lines correspond to effective ordinary and extraordinary optical functions for the fill factor $f = 0.5$, respectively.

3.3 Drude model

Metals and metallic compounds are characterized by strong absorption in visible and infrared spectral range originating from free-electron transitions. The optical functions of metals are usually described using Drude model, which is a simplification of previously introduced DHO model ($E_0 \to 0$). Drude model is in ellipsometric community understood as being basic model describing fundamental properties of metals and its optical function has the form:

$$\epsilon(E) = \epsilon_0 + \frac{A^2}{-E^2 - i\Gamma E}, \tag{8}$$

where A is the plasma energy and Γ is the relaxation. Using EMA formulae from (3) together with Eq. (8) leads to the effective optical functions in the form of Drude formula for the ordinary and DHO for extraordinary case:

$$\epsilon_o(E) = \epsilon_{0,o} + \frac{A_o^2}{-E^2 - i\Gamma_o E}, \tag{9a}$$

$$\epsilon_e(E) = \epsilon_{0,e} + \frac{A_e E_{0,e}^2}{E_{0,e}^2 - E^2 - i\Gamma_e E_{0,e} E}, \tag{9b}$$

where the parameters $\epsilon_{0,o}$, A_o, Γ_o, $\epsilon_{0,e}$, A_e, $E_{0,e}$, and Γ_e are summarized in the fourth column of the Table 1. Figure 6 shows ordinary and extraordinary optical functions of effective grating medium consisting of metallic lamellas described by Drude spectral function and air $\epsilon^{(L)}(E) = 1$ for the fill factor $f = 0.5$. Drude function is described by the chosen parameters $\epsilon_0 = 1$, $A = 5$ eV, and $\Gamma = 0.5$ eV. Similarly as for DHO, the ordinary optical function is rather simple linear combination of the two materials.

Peculiar behavior was found for the extraordinary effective optical function, that exhibits pure DHO behaviour (see Figure 6). As it is shown in Figure 7, a peak appears in the imaginary part of the extraordinary optical function $\epsilon_{2,e}$ and its position strongly depends on the fill factor. Figure 8 shows the oscillator resonance energy $E_{0,e}$ dependence on the fill factor f for extraordinary dielectric function. Maximal shift of DHO resonance energy is obtained for $f \to 0$ asymptotically approaching to $E_{0,e,\max} = A/\sqrt{\epsilon_0}$. Note that from Table 1 the product $\Gamma_e E_{0,e} = \Gamma$ is constant, which means that broadening of the peak remain constant for all fill factors.

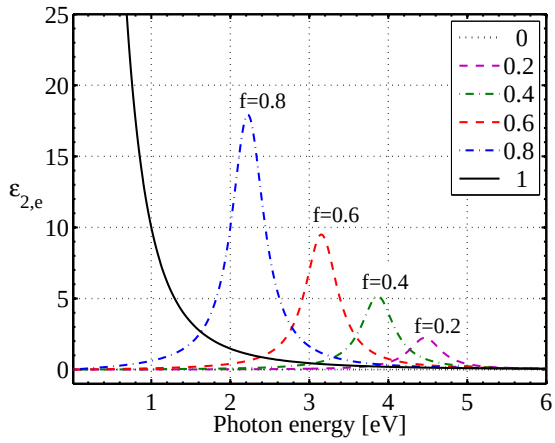

FIG. 7 Imaginary parts of the effective extraordinary optical functions for chosen fill factors for material (8) with parameters $\epsilon_0 = 1$, $A = 5$ eV, and $\Gamma = 0.5$ eV.

This interesting behaviour of the extraordinary effective optical function gives wide possibilities for applications of metallic nanogratings. In the spectral range below 3 eV in Figure 6 the effective optical functions show strong dichroism. For the ordinary wave, the effective nanograting is absorbing as typical for metals. However, the extraordinary wave is not absorbed and nanograting behaves as dielectric-, or semiconductor-like material. Such properties of metallic grat-

ings are already used in infrared polarimetry and ellipsometry for polarizer applications.

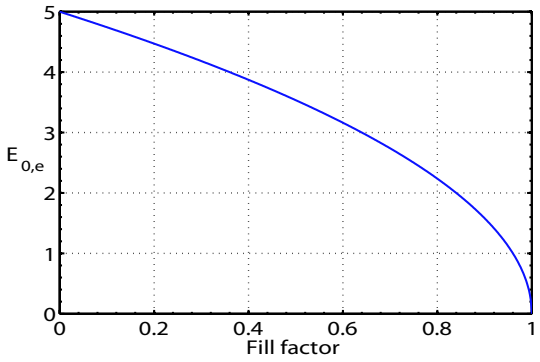

FIG. 8 Dependence of the oscillator energy of the effective extraordinary optical function $E_{0,e}$ on the fill factor ($\epsilon_0 = 1$, $A = 5$ eV, and $\Gamma = 0.5$ eV).

	Sellmeier (5)	DHO (7)	Drude (9)
A_o	Af	Af	$A\sqrt{f}$
$E_{1,o}$	E_1	–	–
$\epsilon_{0,o}$	$f\epsilon_0 + (1-f)$	$f\epsilon_0 + (1-f)$	$f\epsilon_0 + (1-f)$
$E_{0,o}$	–	E_0	–
Γ_o	–	Γ	Γ
A_e	$Af/(\epsilon_{e,1}\epsilon_{e,2})$	$Af/(\epsilon_{e,1}\epsilon_{e,2})$	$f/[(1-f)\epsilon_{e,1}]$
$E_{1,e}$	$E_1\sqrt{\epsilon_{e,2}/\epsilon_{e,1}}$	–	–
$\epsilon_{0,e}$	$\epsilon_0/\epsilon_{e,1}$	$\epsilon_0/\epsilon_{e,1}$	$\epsilon_0/\epsilon_{e,1}$
$E_{0,e}$	–	$E_0\sqrt{\epsilon_{e,2}/\epsilon_{e,1}}$	$A\sqrt{(1-f)/\epsilon_{e,1}}$
Γ_e	–	$\Gamma\sqrt{\epsilon_{e,1}/\epsilon_{e,2}}$	$\Gamma\sqrt{\epsilon_{e,1}/[(1-f)A^2]}$

$$\epsilon_{e,1} = f + (1-f)\epsilon_0, \quad \epsilon_{e,2} = f + (1-f)(A+\epsilon_0)$$

TABLE 1 Parameters of effective spectral optical functions.

4 COMPARISON OF THE EMA WITH RIGOROUS FITS

In the previous section, properties of nanogratings consisting of material described by pure ideal spectral functions were discussed. However, optical functions of natural materials are usually more complex. Often real materials have to be parametrized using advanced models [17] or as a superposition of several basic functions (Sellmeier, DHO, Drude). Even in such cases the ordinary dielectric function can be easily described. However, the extraordinary dielectric function can not be obtain in an analytically closed form.

Simple quasi-static model of EMA given by Eq. (3) is compared with the rigorous effective parameters. The rigorous EMA parameters are obtained by fitting of the Mueller matrix response from an effective layer to the rigorous RCWA model of grating response. Mueller matrix data contain not only information about amplitude of reflected light, but also about phases. That increases sensitivity of the fit to the phase changes and simulate real Mueller-matrix-polarimetry measurements.

The Mueller matrix data are modeled using the RCWA with totally 41 Fourier harmonics (N=20). The precision of the data is sufficient for all modeled cases (see Figure 9 for convergence tests) as the error of the RCWA modeling of the relative Mueller matrix elements is less then 10^{-4}.

The relative Mueller matrix data for the incidence angles ranging from 0° to 85° with step of 5° are simultaneously fitted to the model. The merit function of the fit is described by

$$\chi^2 = \frac{1}{7k-n}\sum_k\sum_{i,j}\frac{1}{\sigma^2}\left(\frac{M_{R,ij,k}}{M_{R,11,k}} - \frac{M_{E,ij,k}}{M_{E,11,k}}\right)^2, \qquad (10)$$

where the indices R and E denote the RCWA and rigorous EMA model and k is the index over all incidence angles. The value of $\sigma = 0.001$ was chosen as an estimate of experimental errors, n denotes number of fitted parameters (two for lossless and four for absorbing cases). Division by the element M_{11} leads to normalized Mueller matrix, which more corresponds to real experiments, where information about the absolute intensity is usually not available. Only seven non-zero elements of Mueller matrix not including M_{11} are used for fitting by the Levenberg-Marquadt algorithm, which also enable to estimate the standard errors of obtained effective parameters (shown in figures as error bars) [18].

The rigorous EMA and the simple quasi-static EMA are compared and validity of this two approaches are discussed including the direct influence of the ration λ/Λ on the precision of description. Even for chosen constant grating period the ratio is rapidly changing in the higher part of the photon energy spectra.

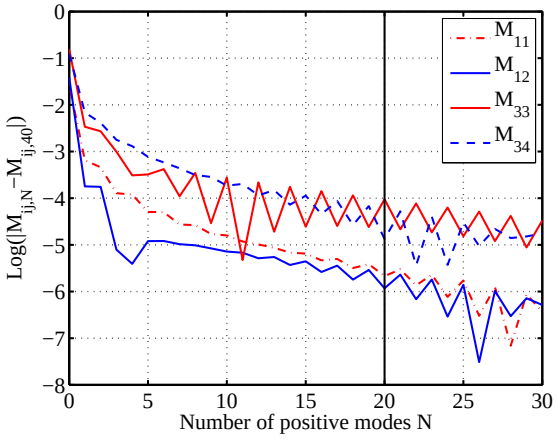

FIG. 9 Convergence of RCWA modeling is shown. Decadic logarithm of Mueller-matrix-elements differences as a functions of number of positive Fourier harmonics in truncated series. In the model we use $N = 20$, which much exceeds usual experimental precision.

General optical properties of nanogratings are discussed on examples of dielectric material (SiO2), semiconductor (silicon), and metal (silver).

4.1 Dielectric material – SiO_2

In this subsection SiO_2 was chosen as grating and substrate material as it represent typical dielectric material. Data of the optical function are taken from Palik handbook [19]. Chosen fill factor is $f = 0.5$ and period of the grating is 20 nm. Thickness of the grating layer is chosen to 200 nm.

Spectral dependence of the effective ordinary and extraordinary optical functions are plotted in Figure 10. Observed good correspondence between the EMA and fitted values for photon energies from 1 to 8 eV ($\Lambda/\lambda < 0.13$) together with the small error bars show that the EMA is very good description for the nanograting. In this range the effective optical functions can be described by simple EMA formulae Eq. (3).

For higher photon energy than 8 eV, SiO_2 becomes absorbing and values of the EMA differ from the fit. This points out, that we are approaching area far from the quasi-static limit. Nevertheless, trend continues with small error bars clearly stating that the grating can be still with good precision described as uniaxial layer for energies below 9.5 eV ($\Lambda/\lambda < 0.16$), but only with non-quasi-static effective values. Figure 11 shows detail of the imaginary part of ε_o, ε_e. Increasing error bars corresponds to increased energy diffracted by higher order Bloch modes.

The effect of instability of the fits due to the breaking of the basic EMA condition is observed for energies higher than 9.5 eV. For given values of permittivity and period the grating is no more describable by only one Bloch mode inside the grating. The fits in the area over 10 eV are much worse and cannot be improved in principle, as the higher order Bloch mode in the grating has significant influence.

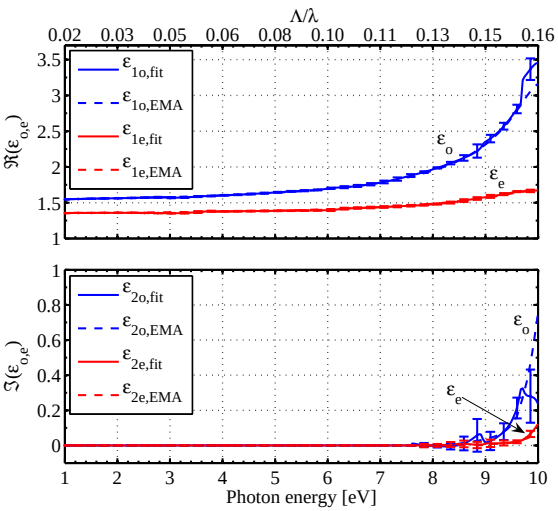

FIG. 10 Effective ordinary and extraordinary optical functions of SiO_2 grating dependent on photon energy. Grating period is $\Lambda = 20$ nm and fill factor is $f = 0.5$. Real and imaginary parts of the fitted and EMA values are plotted with corresponding error bars. The ratios Λ/λ for corresponding photon energies are written on the top of the graph.

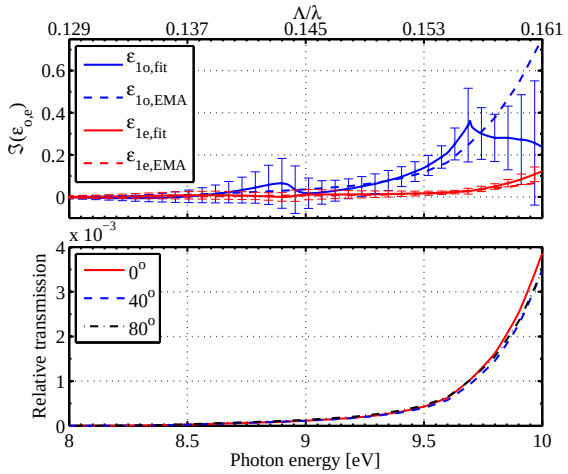

FIG. 11 Upper panel shows detail of Figure 10 for energy range from 8 to 10 eV. Increased error bars corresponds to the energy diffracted to higher order Bloch waves. The lower panel shows sum of TM polarization transmissions of all higher Bloch waves divided by transmission of zero Bloch wave on the interface between incident medium and grating (values for TE polarization are about two orders smaller).

4.2 Semiconductor material – Si

This subsection deals with properties of nanograting composed from silicon as a typical semiconductor material, for which the interband absorption dominates in visible spectral range.

Figure 12 shows strong difference between ordinary and extraordinary effective optical functions.

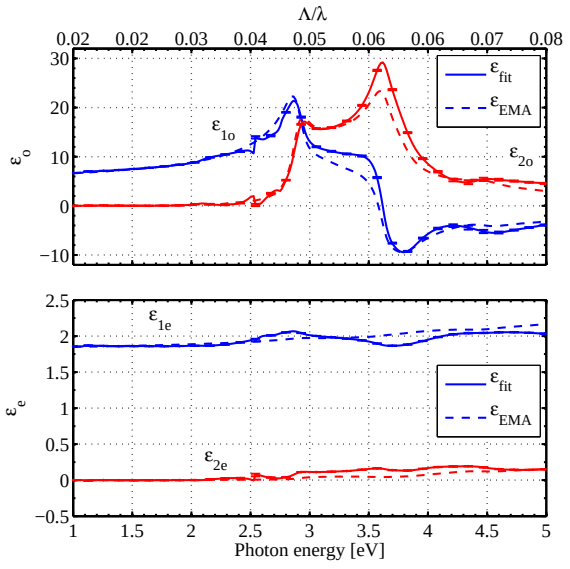

FIG. 12 Effective ordinary and extraordinary optical functions of Si grating as a function of photon energy. Grating period is $\Lambda = 20$ nm and fill factor is $f = 0.5$. Ordinary and extraordinary optical functions are plotted in the top and bottom figure, respectively. Fitted values are plotted with corresponding error bars and compared with simple EMA. The ratios Λ/λ for the corresponding photon energies are plotted on the top of the graph.

The optical functions of Si were taken from Refs. [20, 21]. The fill factor $f = 0.5$, the period $\Lambda = 20$ nm, and the thickness

of the grating layer 200 nm were chosen. Despite the ordinary permittivity copy absorption features, the extraordinary one correspond rather to non-absorbing material. As a consequence, strong dichroism is typical for visible and ultraviolet spectral range for silicon nanograting.

For the photon energies up to 2.5 eV fits the good correspondence between simple EMA and fitted values is observed. With rapid increase of imaginary part of optical function of SiO_2 after 2.5 eV, the differences between the EMA and fit are apparent. Nevertheless, the error bars of the fit remain small, which shows that grating can be still described as effective layer for the rest of showed spectrum, even over the differences between the fit and quasi-static values.

4.3 Noble metal – Ag

In this section silver was chosen as a nanograting material to show effects described in subsection 3.3. Figure 13 shows optical function of silver from Palik handbook [22] used for following model. For the modeling, a 200 nm thick silver nanograting with the period $\Lambda = 20$ nm, fill factor $f = 0.5$, and with silver substrate was chosen.

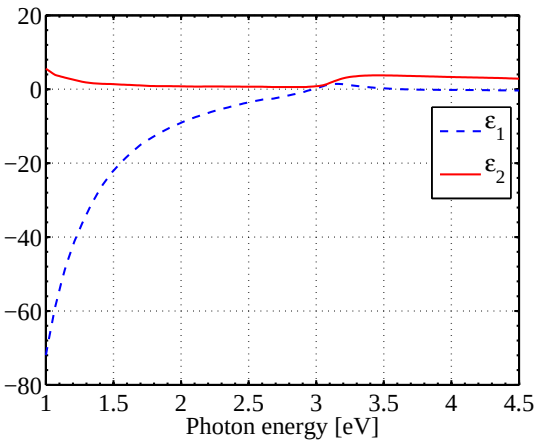

FIG. 13 Optical function of silver used for modeling (from data in [22]).

Figure 14 shows spectral dependence of the effective ordinary and extraordinary functions. Fitted values plotted as solid lines with the corresponding error bars are compared with the quasi-static EMA values denoted by dashed lines. Both approaches are in good correspondence up to energy of 3 eV ($\Lambda/\lambda < 0.05$), where imaginary part of extraordinary optical function ϵ_{2e} starts to grow.

At the energy 3.7 eV, the ϵ_{2e} surprisingly (but in correspondence with previous section) exhibits a peak. This peak is of DHO type as was stated before and its position and amplitude is dependent on the fill factor. Strong dichroism can be found almost at whole spectral range, where for the energies $E < 3$ eV the absorption in ordinary direction is dominant and for energies 3.5 eV $< E <$ 3.8 eV absorption in the extraordinary direction dominates. This property raises wide area of applicability as was mentioned in previous section.

For higher energy than 4 eV ($\Lambda/\lambda \approx 0.07$) the influence of higher order Bloch modes is remarkable and failure of the EMA can be noticed there (indicated by fast increase of the errors of fit).

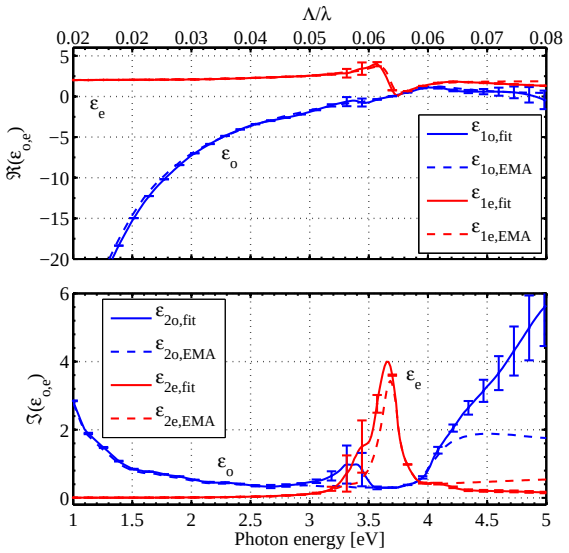

FIG. 14 Effective ordinary and extraordinary optical functions of Ag grating dependent on photon energy. Grating period is $\Lambda = 20$ nm and fill factor is $f = 0.5$. Real and imaginary parts of the fitted and EMA values are plotted with corresponding error bars in top and bottom figure, respectively.

5 CONCLUSIONS

In this article, the spectral dependence of effective parameters of sub-wavelength lamellar grating from materials described by common optical function, namely Sellmeier formula, damped harmonic oscillator, and Drude formulae, was studied. Analytical formulae (5), (7), and (9) describing behaviour of the effective ordinary and extraordinary permittivities in spectral range were derived. Analysis of the imaginary part of extraordinary effective optical function showed high energy shift of DHO absorption peak and also surprising peak appearance for the Drude model.

Effective parameters of the nanogratings consisting of natural materials were obtained from simple EMA (in quasi-static limit) and compared with fit of rigorous data in wide spectral range. As the ratio Λ/λ is increasing, effective medium approximation do not exactly describe optical response of nanograting. This lead to dispersion of parameters over range of the incidence angles, which can be characterized in the fitting procedure by uncertainty of the fitted values. When the uncertainties increase over certain value, the EMA cannot be anymore used for precise description of sub-wavelength gratings. This threshold value of Λ/λ is dependent on the permittivity of the material, where higher permittivity leads to shift to smaller values of the ratio Λ/λ.

Partial support from the project KAN 400100653, MSM6198910016, NANOMAG-LAB project (2004-003177), and from the Grant Agency of the Czech Republic (202/06/0531) is acknowledged.

References

[1] K. Vedam, "Spectroscopic ellipsometry: a historical overview" Thin Solid Films **313-314**, 1–9 (1998).

[2] D. E. Aspnes, "Expanding horizons: new developments in ellipsometry and polarimetry" Thin Solid Films **455–456**, 3–13 (2004).

[3] G. E. Jellison Jr., V. I. Merkulov, A. A. Puretzky, D. B. Geohegan, G. Eres, D. H. Lowndes, and J. B. Caughman, "Characterization of thin-film amorphous semiconductors using spectroscopic ellipsometry" Thin Solid Films **377-378**, 68–73 (2000).

[4] G. P. Nordin and P. C. Deguzman, "Broadband form birefringent quarter-wave plate for the mid-infrared wavelength region" Opt. Express **5**, 163–168 (1999).

[5] R. Haïdar, G. Vincent, N. Guérineau, S. Collin, S. Velghe, and J. Primot, "Wollaston prism-like devices based on blazed dielectric subwavelength gratings" Opt. Express **13**, 9941–9953 (2005).

[6] H. Lajunen, J. Turunen, and J. Tervo, "Design of polarization gratings for broadband illumination" Opt. Express **13**, 3055–3067 (2005).

[7] D. W. Berreman, "Optics in stratified and anisotropic media: 4×4-matrix formulation" J. Opt. Soc. Am. **62**, 502–510 (1972).

[8] K. Rokushima and J. Yamakita, "Analysis of anisotropic dielectric gratings" J. Opt. Soc. Am. **73**, 901–908 (1983).

[9] M. Nevière and E. Popov, *Light Propagation in periodic media: Differential theory and design* (Marcel Dekker, 2002).

[10] M. Born and E. Wolf, *Principles of Optics* (5th edn. Pergamon, Oxford, 1975).

[11] C. W. Haggans, L. Li, and R. K. Kostuk, "Effective-medium theory of zeroth-order lamellar gratings in conical mountings" J. Opt. Soc. Am. A **10**, 2217–2225 (1993).

[12] S. M. Rytov, "Electromagnetic properties of a finely stratified medium" Sov. Phys. JETP **2**, 466–475 (1956).

[13] P. Lalanne and J.-P. Hugonin, "High-order effective-medium theory of subwavelength gratings in classical mounting: application to volume holograms" J. Opt. Soc. Am. A **15**, 1843–1851 (1998).

[14] M. Foldyna, R. Ossikovski, A. D. Martino, B. Drevillon, K. Postava, D. Ciprian, J. Pištora, and K. Watanabe, "Effective medium approximation of anisotropic lamellar nanogratings based on Fourier factorization" Opt. Express **14**, 3114–3128 (2006).

[15] L. Li, "Use of Fourier series in the analysis of discontinuous periodic structures" J. Opt. Soc. Am. A **13**, 1870–1876 (1996).

[16] L. Li, "Formulation and comparison of two recursive matrix algorithms for modeling layered diffraction gratings" J. Opt. Soc. Am. A **13**, 1024–1035 (1996).

[17] M. Foldyna, K. Postava, J. Bouchala, J. Pištora, and T. Yamaguchi, "Model dielectric function of amorphous materials including Urbach tail" Proc. of SPIE **5445**, 301–305 (2004).

[18] W. H. Press, S. A. Teukolsky, W. T. Vetterling, and B. P. Flannery, *Numerical Recipes in C++. The art of scientifique computing* (second edn. Cambridge, 2002).

[19] H. R. Philipp, "Handbook of Optical Constants of Solids" (Academic Press, 1991), chap. Silicon Dioxide (SiO_2) (Glass), p. 771.

[20] D. E. Aspnes, A. A. Studna, and E. Kinsbron, "Dielectric properties of heavily doped crystalline and amorphous silicon from 1.5 to 6.0 eV" Phys. Rev. B **29**, 768 (1984).

[21] E. D. Palik (ed.), *Handbook of Optical Constants of Solids I and II and III* (Academic Press, 1991).

[22] D. W. Lynch and W. R. Hunter, "Handbook of Optical Constants of Solids", (Academic Press, 1991), chap. Comments on the optical constants of metals and an introduction to the several metals, pp. 275–367.